

Rain Reflectivity Distribution and Detectability in Automotive Radar

Henrik Toss¹, Kristian Karlsson¹, Pierre Duthon², Yuri Poledna³

Abstract—In the development of automated driving and advanced driver assistance systems, it is essential that the underlying algorithms are thoroughly tested. Simulation is a valuable tool for evaluation of such algorithms, especially in safety-critical scenarios. Simulations can also provide the opportunity to generate and repeat rare, yet important, test cases and can be applied at various stages of development. For simulation to serve as a reliable substitute for real-world testing, it must offer high fidelity. Therefore, advanced models for both sensors, and the sensed environment are required. A thorough understanding of adverse weather conditions within the operational design domain is consequently crucial to maintain fidelity. This work develops statistical models of radar backscatter from rain for the perception by automotive radars which can be implemented in a simulated environment. To demonstrate the method’s validity, both simulation and real-world data are used to assess the fidelity of rain radar signal predicted or generated using the model. The work presented here offers a state-of-the-art understanding of how rain (based on drop size distributions) affects the radar model and the background signal to be expected across the radar field of view, including the velocity dimension. With the use of such models in simulation it is possible to anticipate how the radar will react in the real-world under similar conditions. Future work includes integrating these findings into a radar-in-the-loop environment and developing additional adverse weather models for radar.

Index Terms—RADAR model, Adverse weather model, Simulation, Measurements, 4D radar, Automated Driving, ADAS.

I. INTRODUCTION

TRAFFIC safety, efficiency and environment are key driving forces in the vehicle industry. One enabler is increasing level of automation through Automated Driving (AD) and Advanced Driver Assistance Systems (ADAS), which rely on sensor input to perceive the surrounding environment. The resulting perception is then forwarded to decision-making algorithms which decide the adequate action in different traffic situations. An AD system has a predefined Operational Design Domain (ODD), which includes aspects such as weather variability [1]. Precipitation is one of many environmental features that may have an impact on driving

conditions as well as sensor performance. It is therefore important to understand how it may affect each sensor function as it impacts systems throughout the AD stack.

Radar is reported to be very robust to weather disturbances as the radar signal attenuation can be considered small over the ranges that are of interest in the automotive context [2]–[5]. However, precipitation is expected to have a detectable radar signature [6], [7], which can contribute to the background noise. This poses a risk of obscuring low-reflectivity targets or confusing the object detection algorithms by the increased clutter levels. Moreover, if it is possible to identify the precipitation and its features from the radar signature, this could also provide valuable input regarding expected driving conditions.

One way to evaluate AD and ADAS functions is through physical testing in all possible weather conditions. However, real-world testing with actual weather disturbances has shown to be difficult, expensive, and time-consuming. Therefore, virtual testing can be used to support and complement this process.

Virtual testing allows for a comprehensive evaluation of the System under test (SUT), in all conditions under the ODD, and even safety-critical scenarios. But for a virtual testing environment to be credible and aligned with the established norms [8], [9], it requires adequate and realistic models, which should preferably be computationally inexpensive to feasibly apply in real-time. When developing such models, it is essential to understand the principles on which the radar works, as well as how the precipitation may affect the signal registered by the radar and how that varies over the field of view (FoV).

Physical testing is still important, and it may be appealing to generate, or emulate, precipitation in some way to reliably and repeatably achieve the desired weather conditions [10]. In that case it is also important to understand the radar working principles as it is not only the position and reflectivity of the drops, but often also their movement, that is registered by the radar sensor.

Data processing and detection algorithms are likely specific to each brand of automotive radar, and the inner workings of the radar is typically not publicly available. The radio wave propagation and principle behind digital beamforming of a receiving antenna array are however general. Through some more high-level information, such as detection limits, FoV, and resolution in different dimensions like range, velocity, and azimuth and elevation angles - combined with

*Co-funded by the European Union. Views and opinions expressed are however those of the author(s) only and do not necessarily reflect those of the European Union or European Climate, Infrastructure and Environment Executive Agency (CINEA). Neither the European Union nor the granting authority can be held responsible for them. Project grant no. 101069576.

¹ RISE – Research Institutes of Sweden, Borås, Sweden. {henrik.toss, kristian.karlsson}@ri.se

² Cerema Centre-Est, Research Team "Intelligent Transport Systems", Clermont-Ferrand, France. pierre.duthon@cerema.fr

³ CARISSMA Institute of Automated Driving, Technische Hochschule Ingolstadt, Ingolstadt, Germany. yuri.poledna@carissma.eu

measurements of radiation patterns - it is possible to make statistical predictions about the effects of precipitation. This work proposes a precipitation radar reflectivity model and describes how it affects the radar signature from the environment across the different dimensions of the detection space. The model is coupled with a simplistic model for a Frequency Modulated Continuous Wave (FMCW) radar - or a similar system - with a digital beamforming array to show the impact on the radar data cube before detection algorithms are applied. In other words, it shows the type of background signal that precipitation would constitute. Finally, the predicted radar signal from the rain is compared to measurements of real-world rain using an automotive radar [11]. Other recent studies have numerically simulated the impact of rain on radar systems [12], [13]. However, these studies present several limitations: they rely on simplified macroscopic models [12], they use proprietary simulation tools with non-public source code [13], do not compare their results with analytical solutions [12], [13], and lack validation of results against real-world data [12], [13]. Our contribution lies in the use of an analytics-based method, with open-source code (available at: <https://github.com/roadview-project/automotive-radar-precipitation-models>), which is subsequently validated against both Monte Carlo-based simulations and real-world measurements.

This work is organized into five sections, the first being the introduction, which opens broad terms on the topic, the second is a deep dive into the theory of the topic and the proposed analytical method, this is followed by a comparison with simulation, a comparison with real-world data, and finally conclusions with a summary of the main findings and a discussion of future research directions.

II. THEORY

The received signal in a modern automotive radar can be broken down into different dimensions, which further can be divided into detection bins. The detectable rain reflectivity in each bin is the sum of the backscattered signals from all raindrops within that bin. Automotive radar typically detects objects based on range, velocity, and angular information (azimuth and elevation). This means the detection space consists of four dimensions in which reflective objects can be distinguished. Assuming the raindrops around the radar adhere to a random uniform distributed in cartesian space, the problem reduces to determining the expected number of drops and typical reflectivity of each 4-dimensional (4D) detection bin.

A. Drop size distribution, velocity and Radar Cross Section

The radar reflectivity of the raindrops is related to their size. As a rough simplification, the falling drops can be assumed to be spherical, with a complex permittivity of $\epsilon_r = 12 - 25i$, at 20°C and the typical automotive radar frequency of 77 GHz, as given in [14]. Using a Mie scattering model [15], the backscattering coefficient can be determined, allowing the Radar Cross Section (RCS) $\sigma(D)$ to be expressed as a function of drop diameter (D), as shown in Fig. 1.

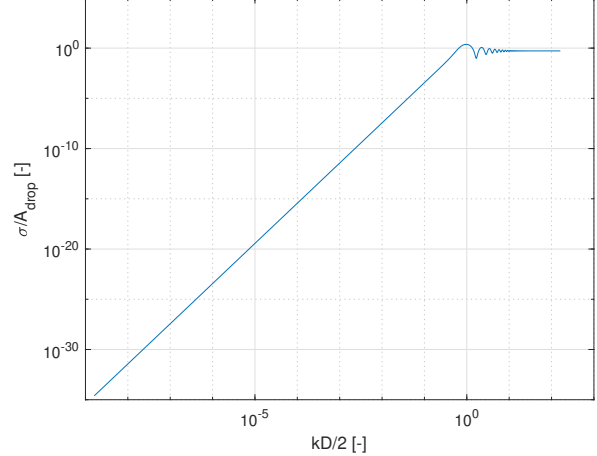


Fig. 1. Function describing relation between diameter D of water droplet and monostatic RCS σ . A_{drop} is the cross-section area of the water drop and k is the wavenumber.

The number of drops ($N(D)$) in a rain fall as well as the distribution of their diameters is often described using the Marshall-Palmer distribution [16],

$$N(D) = N_0 e^{-\Lambda D}, \quad (1)$$

where N_0 and Λ are constants, defined by [16] as $N_0 = 8000 m^{-3} mm^{-1}$ and $\Lambda = 4.1 R^{-0.21} mm^{-1}$, R in this case being the rain rate of the precipitation in mm/h. The total number of drops in a unit volume N_{UV} can be calculated

$$N_{UV} = \int_0^{D_{max}} N_0 e^{-\Lambda D} dD = \frac{N_0}{\Lambda} (1 - e^{-\Lambda D_{max}}), \quad (2)$$

where $D_{max} = 10$ mm is the maximum drop diameter. It is assumed that the rain drops have reached terminal velocity such that the falling velocity $v_{drop}(D)$ of each drop can be determined based on their diameter [17]

$$v_{drop}(D) = a D^b, \quad (3)$$

where $a = 2115 cm^{1-b} s^{-1}$ and $b = 0.8$ are empirical constants.

B. Range (r), Azimuth (θ), and Elevation (ϕ) angles

As the radar measures range it makes sense to inspect the volume of a small range segment dr by simply looking at the surface elements on a sphere with radius r

$$dS_r = r^2 \cos(\varphi) d\theta d\varphi, \quad (4)$$

where θ is the azimuth, φ is the elevation and r is the range. Provided coherent detection, the radar reflectivity of the detection bins is therefore expected to increase with r^2 .

For the detection angles the relative bin size depends on antenna array design and the radar signal processing. For a planar array the dependency will be ill-conditioned for angles close to $\pm\pi/2$. It is not the actual angle that is sensed, but

rather the phase difference of the signal $\Delta\phi$ between the array elements such that

$$\Delta\phi = kd \cdot \hat{r}, \quad (5)$$

where $\mathbf{d} = (0, d_y, d_z)$ describes the distance between antenna elements in the two directions in a rectangular planar array and k is the wavenumber. As it is the projection of the angular vector onto the array plane that is detected, $d\theta, d\varphi$ are thus not constant with θ, φ respectively. Including this projection leads to an indefinite integral and integrating over a known interval of θ, φ to determine the surface element becomes non-trivial. However, as we have assumed a uniform random distribution of the rain, we can, e.g., utilize a quasi-Monte Carlo (QMC) integration method using a spherical Fibonacci point set [18] as an efficient method to estimate the distribution of a limited set of $\Delta\phi$, and from that in turn estimate the distribution over θ, φ where it is not ill-defined (θ, φ close to $\pm\pi/2$).

C. Statistics and near Range

The signal contribution making the round trip from the radar via a single drop and back can be estimated from

$$s_{drop} = C\sqrt{\sigma(D)}e^{-i2kr}r^{-2}, \quad (6)$$

where C is related to the transmit power and antenna gain. The registered signal within a detection bin will be the coherent sum of the signal from every drop in that bin. When $r \gg \Delta r$, where Δr is the range resolution, there will not be much difference in neither the number of drops nor amplitude of the signal coming from those drops over the span of the resolution bin. With a large number of drops the phase of the different contributions to the total signal will thus take on a normal distribution and the expected total amplitude will be Rayleigh distributed. As $s_{drop} \propto r^{-2}$ the detected power $P_{drop} \propto r^{-4}$, while $N \propto r^2$ resulting in a relation of total bin rain detected power $P_{bin} \propto r^{-2}$. The expected value can thus be estimated from the knowledge of the distribution, the mean drop RCS within the bin and the volume of the bin. This is in line with what is reported by [19], [20].

When the range is on the same order of magnitude as the range resolution this reasoning will break down both because of the variation in number of drops over the range, the amplitude, as well as the drops at the closest range, thus more likely to have the largest individual contribution, will also be in phase. Simply calculating the mean of the signal $\langle s \rangle$ over a range bin of width Δr shows that

$$\langle s \rangle \propto (r(r - \Delta r))^{-1} \quad (7)$$

which indicates that the registered signal, at the very shortest distances where $r \sim \Delta r$, should be expected to be higher relative to the bin volume.

D. Velocity

It is only the radial component v_r of the relative velocity of any radar target that is instantaneously registered by the radar, and that can thus be utilized to separate targets that would otherwise be too close to distinguish from each other.

The relative radial component v_r of any target, including raindrops is the scalar product of the total relative velocity projected onto the unit range vector \hat{r}

$$v_r = (\mathbf{v}_{drop} - \mathbf{v}_{radar}) \cdot \hat{r}. \quad (8)$$

Assuming that all drops of the same size D , within a surface element S_r , have approximately the same velocity relative to the radar, the expected distribution of v_r over S_r can be calculated using the same method as described for the QMC integration to generate uniformly distributed points over S_r [18]. This results in the function $p(v_r(D) | S_r)$. The total distribution of RCS over detectable velocity can then be calculated by integration over all drop sizes. Since $|v_{drop}| = v_{drop}(D)$ and the signal power depends on the sum of $\sigma(D)$ for each drop, the expected total signal dependence over velocity expressed as a scaling factor is

$$p(v_r | S_r) = \int_0^{D_{max}} p(v_r(D) | S_r) \frac{N(D) \sigma(D)}{N_{UV} \langle \sigma \rangle} dD. \quad (9)$$

As the projection of the velocity onto the \hat{r} -vector is independent of r , and the signal dependency integral is normalized, (9) can preferably be solved on, e.g., a segment on the unit sphere and then applied as the velocity distribution spread on the mean bin RCS of that segment at any range.

III. COMPARISON WITH SIMULATION

A MATLAB script is developed that generates drops according to the stated Marshall-Palmer distribution with a random uniform distribution in space. The drops are assigned a velocity vector pointing straight downward, with velocity according to [17] and an RCS according to [15]. The algorithm also assumes a monostatic radar with a single isotropic antenna i.e. ignoring the angular bins. Situation specific input parameters needed are rain rate R , range resolution Δr , unambiguous velocity range (v_{min}, v_{max}) and resolution Δv , as well as velocity of the radar sensor itself v_{radar} . Some plausible parameters are chosen as example and shown in Table I.

TABLE I
SIMULATION INPUT PARAMETERS

R [mm/h]	Δr [m]	(v_{min}, v_{max}) [m/s]	Δv [m/s]	v_{radar} [m/s]
11	0.2	(-26.5, 26.5)	$\frac{v_{max} - v_{min}}{512}$	0, 14

The total signal from all drops within a specific range bin is calculated as the coherent sum of the signal s_n from each drop individual drop

$$\sum_N s_n = \frac{\lambda^2}{(4\pi)^3} \left| \sum_N \sqrt{\sigma_n} e^{i\phi_n} r_n^{-2} \right|^2, \quad (10)$$

where

$$\phi_n = 2\pi \frac{2r_n}{\lambda}, \quad (11)$$

and where r_n is the corresponding range to each drop. Random drops are generated this way 500 times and a comparison between analytically derived Cumulative Density

Functions (CDF) at different ranges and the results from calculating the RCS from the simulated receiver signal are plotted together in Fig. 2.

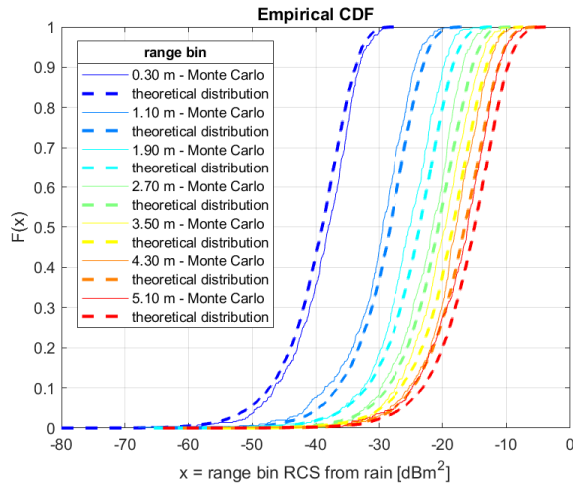


Fig. 2. Empirical CDF:s of range bin RCS for Monte Carlo simulated data together with the analytically derived theoretical distributions for the same ranges, for rain with $R=11$ mm/h.

A curve for the expected value of total RCS of the entire range bin as function of range is plotted in Fig. 3. Fig. 3 also shows curves representing other rain rates to give the reader an indication of what to expect if adjusting this parameter in the model.

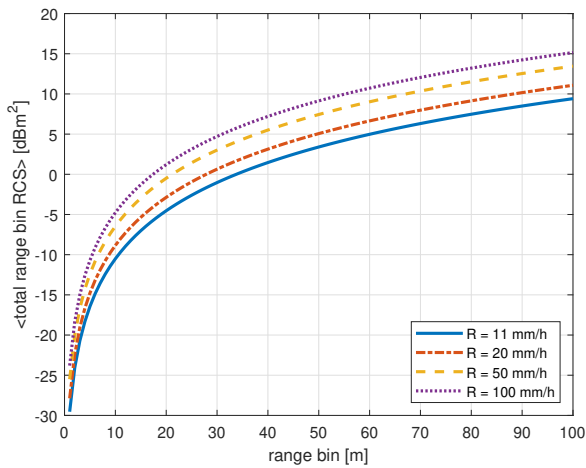


Fig. 3. Expected value of total range bin RCS (i.e., all angles and velocities) due to rain as function of range bin centre. Curves are here presented for four different values of rain rate R to show the increase of rain radar reflectivity with rain intensity

If the signal can be further separated in other dimensions this will still be the expected total RCS, i.e., the sum over all bins in all directions, at the specified range.

By inspecting a specific range bin, the signal can be divided into velocity bins. In Fig. 4 ($v_{radar} = 0$ m/s) and Fig. 5 ($v_{radar} = 14$ m/s) the analytically calculated distribution over velocity bins, of the signal at the specified range, is

plotted together with the coherent sum of the signal from the randomly generated drops at the corresponding range and velocities for one simulated radar frame. The Rayleigh distribution of the total signal applies here as well. The range chosen for the example is 5.1 m and was selected as it is sufficiently large to have a range bin with a volume that makes it likely to find drops in most velocity bins of interest.

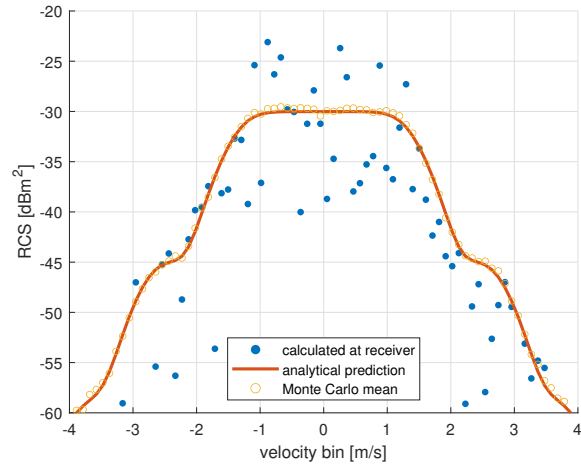


Fig. 4. Velocity bin RCS for $r = 5.1$ m, $v_{radar} = 0$ m/s, $R = 11$ mm/h. Result from one simulated radar frame together with analytically predicted expected value as well as mean over all Monte Carlo simulated radar frames.

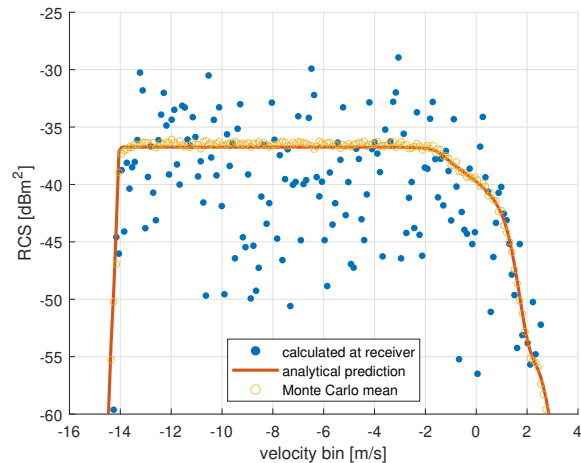


Fig. 5. Velocity bin RCS for $r = 5.1$ m, $v_{radar} = 14$ m/s, $R = 11$ mm/h. Result from one simulated radar frame together with analytically predicted expected value as well as mean over all Monte Carlo simulated radar frames.

The maximum analytical mean RCS in the case where the radar has higher velocity is about 7 dB lower than the stationary case due to being spread out over more velocity bins, and even almost 17.5 dB lower than the calculated total range mean that would be the result without any velocity separation.

A similar effect might be seen for the spread over detection angles in the case of using an antenna array. A tentative map of expected scaling factor based on spread over angles was

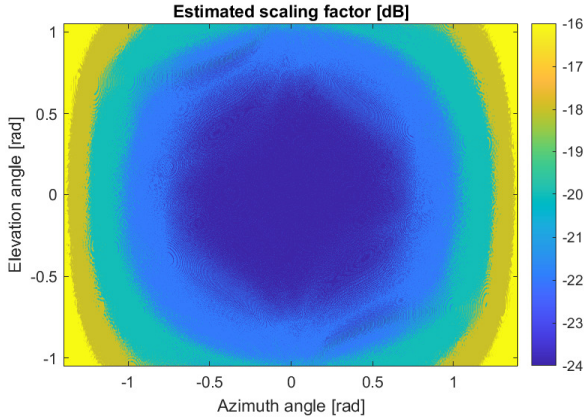


Fig. 6. Estimate of how the compound RCS of the drops in some angular bin would likely scale with color scale in dB. Here the levels are adjusted to reflect a rectangular planar array with 16 by 8 elements.

achieved by oversampling while integrating over a known interval of θ, φ to determine the surface element as a scaling factor representing how the returned signal power is spread over the angular bins followed by re-scaling to reflect how the detected RCS would be expected to scale for a 16 by 8 planar array. Fig. 6 shows the estimated scaling factor for a limited angular FoV. Note that this did not take the antenna patterns into account, and only the effects of the digital beam-steering were accounted for.

It should be noted that the scaling factor over a large part of the FoV is very close to what is expected if simply dividing the entire energy equally, i.e.

$$p(\theta, \varphi) = -10 \log_{10}(K \times L), \quad (12)$$

where $K \times L$ are the number of elements of the array, which in this example case would yield $p \approx -21$ dB. It should also be noted that the scaling factor in Fig. 6 is independent of rain rate.

IV. COMPARISON WITH REAL DATA

As part of the ROADVIEW project [11], an automotive grade radar, with capability to separate targets in 4D, was mounted at an elevated point to achieve a space in front of the radar with very few targets (Fig. 7).

The location of Puy-de-Dôme (France) was chosen for its varied weather conditions, including rain. Data were recorded for intervals of 30s per day, for the entire winter, with a weather station nearby. The detections reported by the radar were recorded during rainfall (as well as in clear weather for control). It was difficult to estimate the rain rate for such a short period of time, however an estimate of 10.5 mm/h was taken as the mean of two different rain rate detectors present in the weather station. The detailed processing of the radar is unknown but based on data provided in the data sheet a qualified guess can be taken. According to the data sheet the antenna array largest physical dimension is

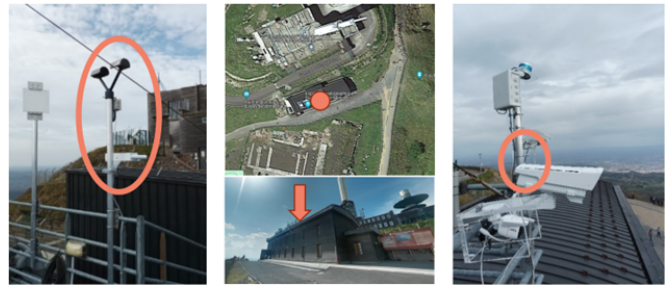


Fig. 7. Presentation of the Puy-de-Dôme site. Right: the radar was installed to capture empty space. Left : the presence of weather sensors to characterize the weather during radar recordings were also visible.

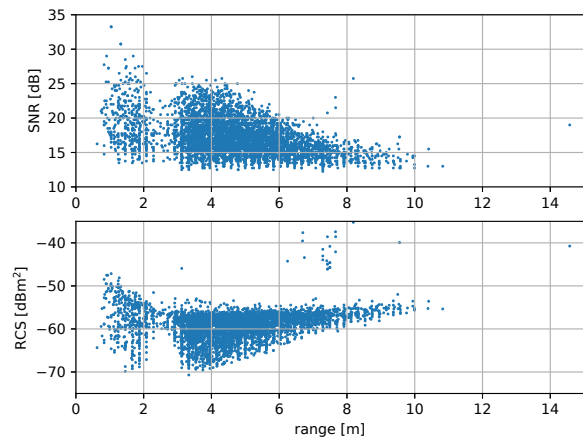


Fig. 8. Accumulated reported detections with detection range on the x-axis. Each point represents one detection reported by the radar. Detection SNR (top) and RCS (bottom)

82 mm. The model thus far has assumed the rain to be at a far field distance. For the given dimension the Fraunhofer limit $d_F = 3.45$ m. At distances shorter than this the electric field component decreases as r^{-2} and the calculated mean would need to be adjusted accordingly. The radar settings used set a maximum range of ~ 100 m divided into 512 equal range bins. The velocity dimension was also divided into 512 equally spaced velocity bins. The velocity range however differs a bit from cycle to cycle, but the total velocity range is $\sim 40 - 50$ m/s. The antenna uses a planar array with a virtual array size of 8 elements along the vertical axis and 16 along the horizontal axis giving a total of 128 elements. It is claimed that a target of 10 dBm^2 can be detected at 350 m, which gives a hint to the signal to noise ratio (SNR) needed for detections to be registered. This means a single undisturbed target with RCS of -52 dBm^2 would be detectable at about 10 m. Figures 8 and 9 show the accumulated detections presented with their SNR and RCS values plotted against range or velocity.

It appears that the radar processing does not quite account for the near field as the RCS appears to be decreasing more rapidly with range at ranges shorter than the Fraunhofer limit. The maximum SNR also decreases with range while

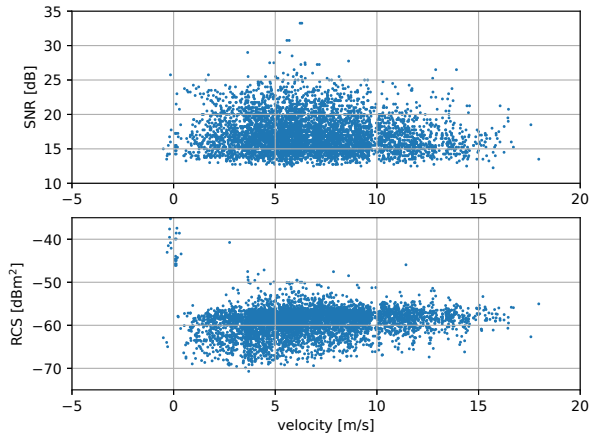


Fig. 9. Accumulated reported detections with detection velocity on the x-axis. Each point represents one detection reported by the radar. Detection SNR (top) and RCS (bottom)

the lower limit for reported detections, as expected, show a more constant behaviour. Since only the bins with an SNR higher than the detection limit will be reported, the distribution functions discussed earlier could be truncated at the corresponding RCS if used only to reflect the statistics of detected rain clutter. The velocity spread differs somewhat from what was predicted in the model. It could very well be speculated that this could be due to strong wind as the sensor is mounted at an elevated location (data from the REHEARSE dataset in the Puy-de-Dome (PDD) is used [11]).

If making the assumption mentioned above that the signal is more or less spread equally over angular bins, and using that scaling factor of -21 dB, we see that the velocity profile in Fig. 9 fairly well matches what is found in Fig. 5 (although the velocity vector appears to be reversed). The difference seen may be due to the antenna diagram which is likely more focused towards the center of FoV giving the slight overestimate by the model.

V. CONCLUSION

The developed model is especially useful in showing how the radar clutter, and background signal originating from rain, differs in behaviour to other noise and clutter when it comes to velocity. It is important to realize that this signal only hints at the distribution of detected rain clutter RCS. In reality, the detection probability is related to the SNR. If only considering the intrinsic sensor noise, it is likely constant over all detection bins. Since the radar signal needs to travel both to and from the reflecting objects, its power will decrease as r^4 while the rain RCS only grows as r^2 , which implies the probability of registering the rain itself as a detection will rapidly decrease with range, even if the rain signal may still slightly affect how other targets are perceived. In a similar way the antenna beam is usually chosen to have its main lobe in the direction of greatest interest, thus increasing the SNR in that region at the cost of decreasing it

in other directions. If the radiation pattern of the antenna is known it may be a good idea to incorporate it in the QMC integral used for calculating the distribution over velocity bins, as it has an angular dependency, and may be preferential if detectability is of greater interest than simply rain RCS. It should be noted that the model only estimates the expected RCS contribution of rain over the detection bins. If using a similar radar model for a driving scenario, where the RCS of more typical traffic targets, such as cars or pedestrians, are simulated separately, a random signal according to this model with random phase could thus be added to the scenario to investigate how harsh weather conditions would impact the scenario. The results presented suggest that the analytical model of radar backscatter statistics provides high fidelity, while being significantly less computationally demanding than simulating the individual behaviour of each raindrop in a scenario.

Future work could therefore be envisaged, in order to carry out this type of scenario in a controlled rain environment and with different targets [10], which would enable us to validate our simulations under these conditions.

ACKNOWLEDGMENTS

The Puy de Dôme (PDD) database is provided by Cerema, and will be available on demand at adweather@cerema.fr. Cerema would like to thank OPGC/LAMP (Clermont-Ferrand Auvergne University) for making the test site available.

REFERENCES

- [1] F. Wang, V. Donzella, P. H. Chan, J. Robinson, Y. Poledna, S. Liandrat, U. Cihan, M. Aramrattana, G. Lee, and E. Erdal Aksoy, "From operational design domain to test cases: a methodology to include harsh weather," *Open Research Europe*, vol. 4, p. 238, Oct. 2024. [Online]. Available: <http://dx.doi.org/10.12688/openreseurope.18592.1>
- [2] N. Balal, G. A. Pinhasi, and Y. Pinhasi, "Atmospheric and fog effects on ultra-wide band radar operating at extremely high frequencies," *Sensors*, vol. 16, no. 5, p. 751, 2016.
- [3] J. Sander, "Rain attenuation of millimeter waves at $\lambda = 5.77, 3.3,$ and 2 mm," *IEEE Transactions on Antennas and Propagation*, vol. 23, no. 2, pp. 213–220, 1975.
- [4] Y. Zhang, A. Carballo, H. Yang, and K. Takeda, "Perception and sensing for autonomous vehicles under adverse weather conditions: A survey," *ISPRS Journal of Photogrammetry and Remote Sensing*, vol. 196, p. 146–177, Feb. 2023. [Online]. Available: <http://dx.doi.org/10.1016/j.isprsjprs.2022.12.021>
- [5] Y. Zhou, L. Liu, H. Zhao, M. López-Benítez, L. Yu, and Y. Yue, "Towards deep radar perception for autonomous driving: Datasets, methods, and challenges," *Sensors*, vol. 22, no. 11, p. 4208, May 2022. [Online]. Available: <http://dx.doi.org/10.3390/s22114208>
- [6] S. Bertoldo, C. Lucianaz, and M. Allegritti, "On the use of a 77 ghz automotive radar as a microwave rain gauge," *Engineering, Technology & Applied Science Research*, vol. 8, no. 1, 2018.
- [7] J. Huang, S. Jiang, and X. Lu, "Rain backscattering properties and effects on the radar performance at mm wave band," *International Journal of Infrared and Millimeter Waves*, vol. 22, pp. 917–922, 2001.
- [8] Economic Commission for Europe, "Proposal for a new un regulation on: Uniform provisions concerning the approval of vehicles with regard to automated lane keeping systems," Economic Commission for Europe, Tech. Rep., 2020.
- [9] Bundesministeriums für Digitales und Verkehr, "Bundesministeriums für digitales und verkehr 86/22," 2022. [Online]. Available: https://www.bundesrat.de/SharedDocs/drucksachen/2022/0001-0100/86-22.pdf?__blob=publicationFile&v=1

- [10] S. Liandrat, P. Duthon, F. Bernardin, A. Ben Daoued, and J.-L. Bicard, "A review of Cerema PAVIN fog & rain platform: from past and back to the future," in *ITS World Congress*, Los Angeles, United States, Sep. 2022. [Online]. Available: <https://hal.archives-ouvertes.fr/hal-03844483>
- [11] Y. Poledna, M. F. Drechsler, V. Donzella, P. H. Chan, P. Duthon, and W. Huber, "Rehearse: adverse weather dataset for sensory noise models," in *2024 IEEE Intelligent Vehicles Symposium (IV)*, 2024, pp. 2451–2457.
- [12] S. Zang, M. Ding, D. Smith, P. Tyler, T. Rakotoarivelo, and M. A. Kaafar, "The impact of adversary weather conditions on autonomous vehicles," *IEEE Vehicular Technology Magazine*, 2019.
- [13] V. Sharma and S. Sergeev, "Range detection assessment of photonic radar under adverse weather perceptions," *Optics Communications*, vol. 472, p. 125891, 04 2020.
- [14] J. H. Jiang and D. L. Wu, "Ice and water permittivities for millimeter and sub-millimeter remote sensing applications," *Atmospheric Science Letters*, vol. 5, no. 7, pp. 146–151, November 2004.
- [15] C. F. Bohren and D. R. Huffman, *Absorption and Scattering of Light by Small Particles*. New York: Wiley, 1983.
- [16] J. S. Marshall and W. M. K. Palmer, "The distribution of raindrops with size," *Journal of Atmospheric Sciences*, vol. 5, no. 4, pp. 165–166, 1948.
- [17] D. Koutsoyiannis and A. Langousis, *Treatise on Water Science Chapter 27: Precipitation*. Elsevier, 2011, vol. 2, pp. 27–78.
- [18] R. Marques, C. Bouville, M. Ribardiere, L. P. Santos, and K. Bouatouch, "Spherical fibonacci point sets for illumination integrals," *Computer Graphics Forum*, vol. 32, no. 8, pp. 134–143, December 2013.
- [19] R. Gourova, O. Krasnov, and A. Yarovoy, "Analysis of rain clutter detections in commercial 77 ghz automotive radar," in *2017 European Radar Conference (EURAD)*, Nuremberg, Germany, 2017, pp. 25–28.
- [20] B. Yang, K. Wu, Z. Guo, and Z. Huang, "Analysis of rain effects on millimeter wave fuze ground-echo characteristics," *Journal of Physics: Conference Series*, vol. 2478, no. 12, p. 122064, June 2023.